

# Spherical Correlation of Visual Representations for 3D Model Retrieval

Ameesh Makadia · Kostas Daniilidis

the date of receipt and acceptance should be inserted later

**Abstract** In recent years we have seen a tremendous growth in the amount of freely available 3D content, in part due to breakthroughs for 3D model design and acquisition. For example, advances in range sensor technology and design software have dramatically reduced the manual labor required to construct 3D models. As collections of 3D content continue to grow rapidly, the ability to perform fast and accurate retrieval from a database of models has become a necessity.

At the core of this retrieval task is the fundamental challenge of defining and evaluating similarity between 3D shapes. Some effective methods dealing with this challenge consider similarity measures based on the visual appearance of models. While collections of rendered images are discriminative for retrieval tasks, such representations come with a few inherent limitations such as restrictions in the image viewpoint sampling and high computational costs. In this paper we present a novel algorithm for model similarity that addresses these issues. Our proposed method exploits techniques from spherical signal processing to efficiently evaluate a visual similarity measure between models. Extensive evaluations on multiple datasets are provided.

**Keywords** 3D shape retrieval · Visual similarity · Spherical Fourier transform

---

Ameesh Makadia  
Google Research New York, New York, NY 10011  
E-mail: makadia@google.com

Kostas Daniilidis  
Department of Computer Science  
University of Pennsylvania, Philadelphia, PA 19104  
E-mail: kostas@cis.upenn.edu

## 1 Introduction

Laser-scanned objects, CAD models, and even image-based reconstructions are just a few of the sources contributing to rapidly growing, publicly available 3D model collections. Along with these vast 3D collections comes the need for a fast, large-scale model retrieval and matching system.

At the core of any content-based model retrieval engine lies the challenge of computing 3D shape similarity. Many of the difficulties in this task can be identified as either *global* or *local*. Any shape representation or similarity measure must compensate for global variations such as change in scale, orientation, etc. The second big challenge lies in local variations caused by object articulations or perturbations to local surface geometry. Such variations can be attributed to noise or even modeling technology. For example, a polygonal mesh obtained from laser data will be quite different from a polygonal model of the same object designed by a human.

3D shape matching for retrieval has been a topic of ongoing research leading to many interesting techniques [1–11], all of which address the challenges mentioned above to various degrees. In this work we are inspired by the family of methods which compare 3D models based on their *visual* similarity [1, 9]. For example, [1] has shown state-of-the-art retrieval and classification results on standard benchmarks. The premise behind this approach is a 3D model representation consisting of a collection of images rendered from various viewpoints. Although it may be a bit surprising that a collection of 2D images provides better discrimination than features based on 3D geometric information, a closer look will reveal two possible reasons for the strength of visual representations. First, rendering

views of a model circumvents the problem of dealing with complex, noisy, and possibly corrupt local 3D surface geometry. Second, if two categories of 3D models can be differentiated even by one particular discriminative view, a sufficient sampling of renderings is likely to capture this distinguishing information.

However, despite their high performance relative to other retrieval methods, the image-based methods present their own challenges and limitations. For example, the Light Field Descriptor (LFD) of [1] is a representation that is not invariant to model orientation. Thus, there is a high computational cost that comes with evaluating a distance measure for many possible rotational alignments between models.

The inspiring idea of our work has first been drafted in [12], where a very preliminary formulation was developed. In this paper we present methods for 3D shape comparison and retrieval that are built upon a visual representation of models. Specifically, similar to [1], our representation is a collection of silhouette images rendered from various viewpoints on the sphere surrounding the model. We define model similarity as the cross-correlation of these rendered silhouette image collections. Our primary contributions are in the formulation and efficient evaluation of this cross-correlation similarity measure. We will show how model similarity can be evaluated efficiently using techniques from spherical harmonic analysis, taking advantage of the fact that spherical correlation is equivalent to multiplication in the spherical Fourier domain. Furthermore, our model comparison method can be extended in a simple and intuitive way to develop an iterative, coarse-to-fine model retrieval system for large collections of models. A thorough experimental evaluation of our proposed methods is presented for multiple challenging datasets, and the results show consistently state-of-the-art or near-state-of-the-art performance.

## 2 Prior work

Content-based 3D model retrieval continues to be an important practical as well as fundamental problem. From the practical perspective, many large web repositories (e.g. 3D Warehouse<sup>1</sup>) ignore shape content for model search, which often leads to search results of limited success and applicability. Many researchers have proposed to address the problem of 3D similarity for the task of model retrieval, and what follows is a brief overview of just a few of the existing methods in the literature.

Global spherical representations are the most natural (and common) representations for 3D models. The

Extended Gaussian Image (EGI, [7]) was perhaps the earliest such representation, but there exist many others such as the Complex EGI [6], spherical distributions of shape area [5], radial distance functions [3, 4], and the Light Field Descriptor [1], just to name a few. Less common is the case where the underlying representation is a 3D grid (see [2, 13] for examples). A large subset of methods based on spherical representations utilize a Spherical Fourier representation to build model descriptors (see [2, 4] for examples).

On the opposite end of the spectrum exist those methods where 3D shapes are represented by local features. Spin images [14, 15] and 3D Shape Contexts [16–18] are examples where surface points are described by shape distributions of a local neighborhood. While local descriptors make it easier to deal with object articulations or missing parts, there is the added challenge of obtaining accurate correspondences. Recently [9] incorporated local SIFT features [19] from rendered depth images into a traditional document retrieval bag-of-features approach to circumvent the direct correspondence problem.

One of the challenges for shape matching is the wide variety of transformations that must be accounted for when comparing 3D models. In this regard, most of the approaches we have mentioned above can be divided into two categories. The first category contains those approaches where invariance to the possible transformations are built directly into the model representation or the extracted descriptors. The second category contains those approaches that address the possible transformations of a model at the time when model descriptors are being compared. For example, the most common transformations to which any 3D retrieval engine must be invariant are global changes in size (scale), position (3D translation), and orientation (3D rotation). Most of the approaches we have discussed above propose methods to generate 3D model descriptors which have built-in invariances (i.e. any scaling, translation, or rotation of the 3D model will not alter the resulting model feature descriptor). There are a number of ways this can be achieved. The most direct is to use descriptors that are inherently invariant to such transformations. For example, histograms of distances between point pairs [8], or histograms of distances from surface points to the center of mass [5], are invariant to both rotation and translation. For those methods where the underlying representation is not invariant to certain transformations, simple measures can be taken: Scale can be normalized by isotropic scaling of a model to fix the average distance from surface points to the center of mass, for example. Translation can be normalized by shifting the model so that the center of mass

<sup>1</sup> <http://sketchup.google.com/3dwarehouse/>

aligns with the origin. A simple way to factor out orientation is to use PCA-alignment, where the principal axes of a model are aligned with some common reference frame. This type of PCA-alignment is commonly used for spherical or 3D grid representations where the model orientation is difficult to factor out. For spherical representations, an alternative to PCA-alignment is to extract general properties of a spherical function that are invariant to 3D rotations. For example, it is well-known that the magnitudes of Spherical Fourier coefficient vectors are invariant to rotation (see [2] for an application to 3D model comparison).

The benefit of encoding transformation invariance into 3D model descriptors is that such features can be directly compared using traditional distance measures. Nearest neighbor retrieval over thousands of models is still a fairly efficient computation when the pairwise distance measure is the  $L_2$  distance between small feature vectors, for example. Furthermore, it is straightforward to utilize powerful classification machinery (e.g. an SVM classifier) with such features.

The problem with encoding invariance directly into the descriptors is that it often comes at a cost. As a general rule, the more invariance captured by a feature the less discriminative the descriptor. Another problem comes from possible inaccuracies in the methods. For example, orientation normalization using PCA-alignment has been shown to be inaccurate [20]. The alternative to building invariant descriptors is to address possible model transformations at the time of similarity (or distance) computation. This allows one the freedom to build very robust and discriminative features from 3D models. However, the penalty is that there is a computational disadvantage when descriptors are compared since the possible transformations must be accounted for. Typically this is addressed by an optimization or search over transformation parameters. For example, the Light Field Descriptor [1] represents a 3D model with a collection of rendered silhouette images. When two models are compared their respective silhouette collections must be compared for all possible 3D rotational alignments.

As our work in this paper builds on a visual model representation, it is closely related to the Light Field Descriptor of [1]. Thus, in the following section we will summarize the approach of [1] and highlight some of the existing limitations which are addressed in this paper.

### 3 Light Field Descriptors (LFD)

The method of [1] can be described as having three steps: First, given a 3D model, a collection of silhou-

ette images are rendered from multiple viewpoints surrounding the model. Second, features are extracted for each image. These features are used for pairwise comparison of images. Third, for the comparison of two 3D models, the pairwise distances between the models' respective image collections are aggregated to provide a composite distance. This computation is then repeated for multiple rotations, and the minimum composite distance is selected as the final distance between the models. In the following subsections we will attempt to fill in many of the details of this approach.

#### 3.1 Silhouette viewpoints

There are a few constraints which help determine the viewpoints from which silhouette images are rendered given a 3D model. Ideally, the viewpoints should be distributed "uniformly" over the sphere, to limit redundancy. Furthermore, the silhouettes from two different models will be compared pairwise for a set of 3D rotations. This implies that there must exist some 3D rotations which map any viewpoint onto another (transitivity), while also mapping the collection onto itself. For a collection of  $N$  viewpoints ( $N > 2$ ), the set of rotations that satisfy this constraint make up a finite subgroup of the 3D rotation group  $SO(3)$ . The finite subgroups of  $SO(3)$  are the cyclic groups, the dihedral groups, and the symmetry groups of the Platonic solids [21]. Although the cyclic and dihedral groups do not limit the number of silhouette vertices, the corresponding rotations will cover only a small subspace of  $SO(3)$ . The Platonic solid with the most vertices is the regular dodecahedron (20 vertices). The dodecahedral group (often referred to by its dual, the icosahedral group), has order 60. In other words, for the configuration of 20 vertices aligned with the vertices of a dodecahedron, there are 60 unique 3D rotations which will map this set of 20 vertices onto itself. We should note that in practice only 10 silhouettes are used since vertices  $p$  and  $-p$  provide identical information. The collection of 10 silhouettes, along with their individual silhouette descriptors, constitute the Light Field Descriptor. A denser sampling of the viewpoint space is obtained by replicating the constellation of 10 silhouettes at small rotational offsets from the initial position.

#### 3.2 Silhouette descriptors

A rendered silhouette image is a binary image with a single connected component. Lacking any appearance information, purely shape-based descriptors are used for the comparison of silhouettes.

The Zernike moment descriptor is obtained by projecting the 2D silhouette onto a set of circular, complex Zernike polynomials of increasing degree. A few examples of Zernike polynomials are shown in figure 1.

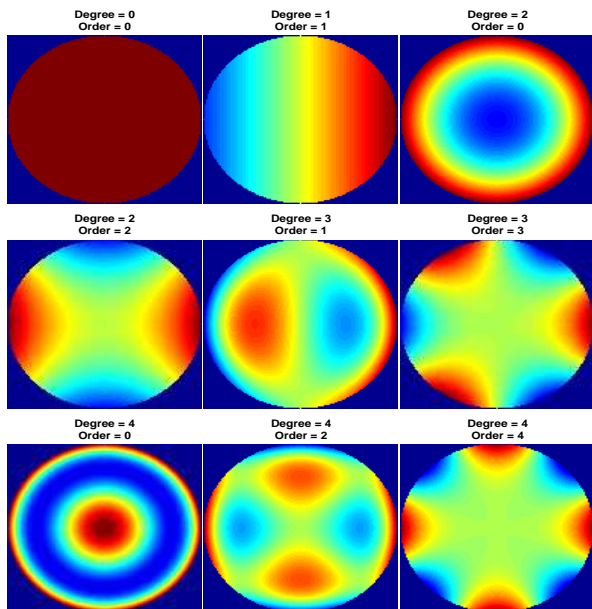


**Fig. 1** Nine Zernike polynomials (see [22] for details). The polynomials are shown for various degrees and orders. The polynomials are complex, so we are only showing the real component here. Colors closer to red are higher values (positive), while colors closer to blue are lower values (negative). The polynomials are defined on the circle, so the region outside the circle should not be considered. The  $(0, 0)$  polynomial is uniform since a projection onto this is equivalent to just an integration of the input function over the circle.

In total, the magnitude of 35 coefficients are kept for the descriptor.

The contour distance function  $r(\theta)$  measures the distance from the silhouette centroid to the contour. An example of a silhouette image along with its extracted contour and corresponding distance function are shown in figure 2.

Since  $r(\theta)$  is a periodic function on the circle, it is natural to examine its Fourier transform  $\hat{r}(k)$ . The magnitude of 10 coefficients are retained for the descriptor.

Both the Zernike moment descriptor and the contour distance descriptor were evaluated extensively in [22], where it was shown an integrated approach utilizing both descriptors performed well for image retrieval tasks.

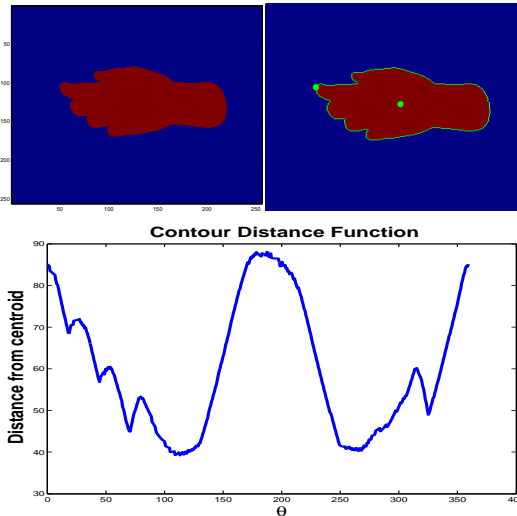


**Fig. 2** On the top left is a sample silhouette obtained from rendering a 3D model of a human hand. On the top right we show the detected contour (obtained by a tracing algorithm) in green. The centroid of the shape is given by the green circle in the middle of the hand. The green circle intersecting the shape contour specifies the first detected point along the contour, which also acts as the starting reference point for generating the contour distance function. The resulting contour distance function, measuring the distance of the contour points to the centroid, is shown in the bottom plot.

### 3.3 Model comparison

Given Light Field Descriptors for two models, there are 60 possible rotational alignments that must be considered. The final 3D model distance is the minimum distance over all Light Field Descriptor pairs for all possible rotational alignments.

To speed up comparisons and retrieval from large databases, a multi-stage comparison approach is proposed in [1]. There are four controllable parameters: (versus accuracy):

1. *Number of silhouettes.* The number of images (up to ten) used in the comparison can be varied.
2. *Number of LFDs can be varied.*
3. *Quantization of silhouette descriptors.* Feature vectors can be quantized so that each coefficient is represented with 4 or 8 bits, for example.
4. *Subset of feature vectors.* Distances can be computed using a subset of the feature vector coefficients.

At each stage of the iterative model comparison, the above parameters are varied to provide additional accuracy, the basic idea being many models can be discarded after each iteration. For details of the proposed six-stage retrieval process see [1].

### 3.4 Limitations

The viewpoint configuration described above is tightly coupled with the set of possible rotational alignments. It is not simple to vary the number or position of viewpoints, or the number or samples of 3D rotations independently. For example, increasing the number of rotational alignments evaluated while keeping the silhouette viewpoints fixed implies silhouette (or feature) interpolation, however there is no clear approach for this.

The full comparison, even for just 100 silhouettes per model, is too computationally expensive for a database search. However, the proposed six-iteration method is fairly complex and seems a bit ad-hoc and arbitrary. There does not exist a clear intuition behind the decisions made during each stage. Combined with an absence of a thorough evaluation, the motivations behind this process, along with the performance contributions from each parameter, are unclear.

Inspired by the discriminative strength of visual model representations, we present our model comparison technique and address the key issues discussed above in the following sections.

## 4 Efficient 3D model comparison

In this section we will detail our proposed 3D model comparison technique. The outline is as follows: In section 4.1, we describe silhouette generation and feature extraction. In section 4.2 we will define a similarity measure for comparing two models, and in 4.3 we show how this similarity measure can be evaluated efficiently borrowing techniques from spherical harmonic analysis. Section 4.4 covers the sampling requirements of our approach. In sections 4.5 and 4.6 we summarize the algorithm and provide some analysis and observations.

### 4.1 Silhouette rendering and feature extraction

Our 3D model representation is a collection of silhouette images rendered from viewpoints surrounding the model. Consider a 3D model centered at the origin. For any sphere point  $p \in S^2$ , we can render a silhouette via an orthographic projection of the model onto the plane tangent to the sphere at  $p$ . In this way we generate silhouette images for any collection of spherical coordinates (we will discuss the number of silhouettes and their locations in subsequent sections). Furthermore, each silhouette we obtain will be represented by a feature vector describing its shape. Although we have a

flexibility in selecting this feature vector, for comparison we will use the 45-dimensional Zernike and contour descriptor as in [1].

### 4.2 Similarity measure

For the moment, let us consider that our collection of silhouettes is not finite, but rather we have obtained images and feature vectors from all points on the sphere. In this continuous setting, we have a  $N$ -dimensional feature vector at each point on the sphere (as described above, in our experiments  $N = 45$ ). Formally, we will write this silhouette feature representation as  $M(p)_i$ , where  $p$  is a sphere point ( $p \in S^2$ ) and  $i$  is the index into the  $N$ -dimensional feature vector that describes the silhouette obtained from viewpoint  $p$ . To compare two 3D models, we define their similarity as the cross-correlation of their feature representations:

$$G_c = \sum_{i=1}^N \left[ \int_{p \in S^2} M_1(p)_i M_2(p)_i dp \right] \quad (1)$$

In practice we evaluate a normalized cross-correlation, but for simplicity we leave out the normalization terms in our description here. Note, equation 1 evaluates a similarity measure over the two model representations  $M_1$  and  $M_2$  in their native orientations. However, as we do not know the correct rotational alignment, we must consider all possibilities:

$$G_c(R) = \sum_{i=1}^N \left[ \int_{p \in S^2} M_1(p)_i M_2(R^T p)_i dp \right], R \in SO(3) \quad (2)$$

Here  $G_c(R)$  measures the cross-correlation for all possible 3D rotational alignments  $R \in SO(3)$ . We define the similarity between two models as the maximum value of  $G_c(R)$ . Computationally, evaluating  $G_c(R)$  directly is cumbersome. For each 3D rotation we must rotate one model representation ( $M_2$ ) and perform a 3D integration. In the next subsections we see how to evaluate  $G_c(R)$  efficiently.

### 4.3 Similarity evaluation

To efficiently evaluate the model similarity function  $G_c(R)$  from equation 2, we recognize that the inner integral fits the definition of a correlation between functions defined on the sphere. Isolating the inner integral gives

$$G(R) = \int_{p \in S^2} M_1(p) M_2(R^T p) dp, R \in SO(3) \quad (3)$$

To evaluate  $G(R)$ , we adopt an approach similar to those described in [23–28], which show that the spherical correlation integral is equivalent to a multiplication

of Fourier transforms. We provide a brief summary of this result here, but readers are referred to [24, 25] for reference.

In traditional Fourier analysis, periodic functions on the line (or equivalently functions on the circle  $S^1$ ), are expanded in a basis spanned by the Eigenfunctions of the Laplacian. Similarly, the Eigenfunctions of the spherical Laplacian provide a basis for  $M(p) \in \mathcal{L}^2(S^2)$  (here  $\mathcal{L}^2$  denotes square-integrability). These Eigenfunctions are the well known spherical harmonics ( $Y_m^l : S^2 \mapsto \mathbb{C}$ ), which form an Eigenspace of harmonic homogeneous polynomials of dimension  $2l+1$ . Thus, the  $2l+1$  spherical harmonics for each  $l \geq 0$  form an orthonormal basis for any  $M(p) \in \mathcal{L}^2(S^2)$ . The spherical harmonic for degree  $l$  and order  $m$  ( $l \geq 0, |m| \leq l, l, m \in \mathbb{Z}$ ), is given as

$$Y_m^l(\theta, \phi) = (-1)^m \sqrt{\frac{(2l+1)(l-m)!}{4\pi(l+m)!}} P_m^l(\cos \theta) e^{im\phi}$$

Note we are using  $p$  and  $(\theta, \phi)$  interchangeably to denote points on the sphere. In the above equation  $P_m^l$  are the associated Legendre functions and the normalization factor is chosen to satisfy the orthogonality constraint. Readers are referred to [29, 30] for an in-depth treatment of spherical harmonics. Any function  $M(p) \in \mathcal{L}^2(S^2)$  can be expanded in a basis of spherical harmonics:

$$M(p) = \sum_{l \in \mathbb{N}} \sum_{m=-l}^l \hat{M}_m^l Y_m^l(p) \quad (4)$$

$$\hat{M}_m^l = \int_{p \in S^2} M(p) \overline{Y_m^l(p)} dp \quad (5)$$

The  $\hat{M}_m^l$  are the coefficients of the Spherical Fourier Transform (SFT). Henceforth, we will use  $\hat{M}^l$  to annotate vectors in  $\mathbb{C}^{2l+1}$  containing all coefficients of degree  $l$ , ordered from  $-l$  through  $+l$ .

As functions on the sphere can be expanded in spherical harmonics, functions defined on the rotation group can be expanded in the irreducible unitary representations of the rotation group. For  $G(R) \in \mathcal{L}^2(SO(3))$ , we can write its Fourier expansion as

$$G(R) = \sum_{l \in \mathbb{N}} \sum_{m=-l}^l \sum_{k=-l}^l \hat{G}_{mk}^l U_{mk}^l(R) \quad (6)$$

$$\hat{G}_{mk}^l = \int_{R \in SO(3)} G(R) \overline{U_{mk}^l(R)} dR \quad (7)$$

The  $\hat{G}_{mk}^l$ , with  $m, k = -l, \dots, l$  are the  $(2l+1) \times (2l+1)$  coefficients of degree  $l$  of the  $SO(3)$  Fourier transform. The  $U_{mk}^l(R)$  are the elements of the irreducible matrix representations of  $SO(3)$ . We will write  $U^l(R)$  for the  $(2l+1) \times (2l+1)$  matrix representation at degree

$l$ , and  $\hat{G}^l$  for the matrix of  $SO(3)$  Fourier coefficients at degree  $l$ .

There is a close relationship between the Fourier representation of functions on the sphere and the matrix representations  $U^l(R)$ . Specifically, as spherical functions are rotated by elements of  $SO(3)$ , their Fourier coefficients are “modulated” by the irreducible representations of  $SO(3)$ :

$$M(p) \mapsto M(R^T p) \iff \hat{M}^l \mapsto U^l(R)^T \hat{M}^l \quad (8)$$

This relationship, along with the orthogonality of the spherical harmonics, allows us to expand equation 3 in terms of the corresponding Fourier transforms:

$$\hat{G}^l = \hat{M}_1^l \overline{(\hat{M}_2^l)^T} \quad (9)$$

This shows that the  $SO(3)$  Fourier coefficients of  $G(R)$  can be obtained as a matrix product between the coefficient vectors of the two spherical functions  $M_1$  and  $M_2$ .

#### 4.4 Viewpoint sampling

A fast discrete algorithm for the spherical Fourier transform, based on a separation of variables technique, can be attributed to [30]. The complexity of the transform is  $O(L^2 \log^2 L)$ , where  $L$  is the “bandwidth” of the spherical function. In practice, the selection of  $L$  simply specifies that only those coefficients of degree *less than*  $L$  will be retained from the Fourier transform. The sampling requirement to achieve the noted complexity is that  $2L$  samples must be placed uniformly in each spherical coordinate (i.e.  $2L$  samples in colatitude, and  $2L$  samples in azimuth). Figure 3 shows the effect of this sampling constraint on the distribution of spherical silhouette viewpoints.

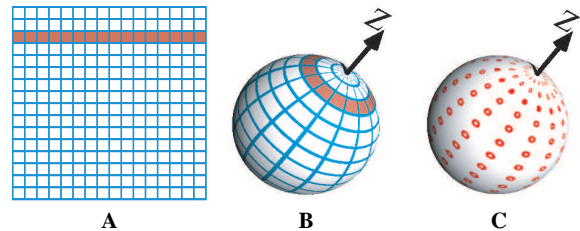


**Fig. 3** On the left (A) is a representation of a uniformly sampled spherical grid, with 16 samples spaced uniformly in each dimension. This is the sampling requirement for a fast spherical Fourier transform at bandwidth  $L = 8$ . (B) depicts the corresponding sample support regions as they appear on the sphere. The highlighted bins correspond to the highlighted row in (A). The circles in (C) specify the actual sample locations on the sphere.

Similar to the spherical transform, there exists a separation of variables technique for a fast discrete  $SO(3)$  Fourier transform [24]. The complexity for such a technique is  $O(L^3 \log^2 L)$ , where as before  $L$  is the function bandwidth. This fast discrete transform is given for a standard Euler angle parameterization of  $SO(3)$ . In particular, the three angles  $\alpha, \gamma \in [0, 2\pi)$  and  $\beta \in [0, \pi]$ , can generate any 3D rotation through  $R = R_z(\gamma)R_y(\beta)R_x(\alpha)$ . Here  $R_z$  and  $R_y$  represent rotations about the  $Z$  and  $Y$  axis, respectively.

For a fast discrete  $SO(3)$  transform of a function with bandwidth  $L$ , the sampling theorem requires  $2L$  samples uniformly spaced in each of the three Euler angles  $\alpha, \beta$ , and  $\gamma$ . As with the spherical transform, this uniform sampling in Euler angles leads to a non-uniform sampling in rotation space.

The fast spherical and rotational Fourier transforms detailed in [24, 30] provide us the machinery necessary for evaluating the spherical correlation integral (equation 3) in the Fourier domain (equation 9).

#### 4.5 Pairwise model comparison summary

We now summarize our pairwise 3D shape comparison formulation as detailed above, and provide some practical considerations and complexity analysis. The only parameter we need to set is the frequency bandwidth  $L$ , which will initially dictate the sampling frequency in the silhouette viewpoint space, as well as the 3D rotation space.

Given two models which we wish to compare, the first step is generating silhouette images and features from each model. As per the Fourier sampling theorem, given a bandwidth  $L$ , we will need to generate  $2L \times 2L = 4L^2$  orthographically rendered silhouette images from each model. For any silhouette viewpoint  $p \in S^2$ , the antipodal point  $-p$  provides redundant information. Thus in practice, we only need to render half the silhouettes (a total of  $2L^2$  images). Figure 4 provides an example of a 3D model and its silhouette images. Subsequently, each silhouette image is replaced with its  $N$ -dimensional feature vector representation. After feature extraction, we have our initial model representations  $M_1(p)_i$  and  $M_2(p)_i$ .

To obtain the Fourier domain representation of  $M(p)_i$ , we must take a separate spherical Fourier transform for each silhouette feature index  $i = 1, \dots, N$ , leaving us with the coefficients  $(\hat{M}_m^l)_i$ . For a fixed  $L$ , we will have a total of  $NL^2$  Fourier coefficients. As we observed earlier, the spherical model representation exhibits the even property  $M(p)_i = M(-p)_i$ . This redundancy translates to the Fourier space:  $(\hat{M}_m^l)_i = 0, \forall l$  odd. Additionally, the spherical Fourier transform

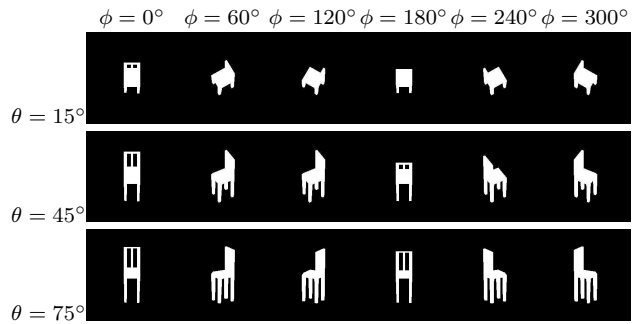
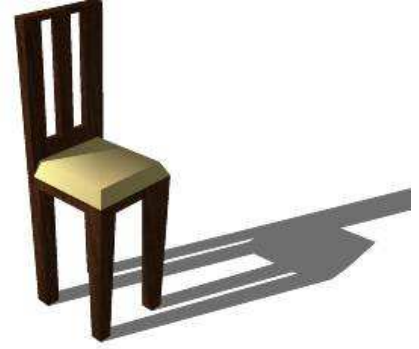


**Fig. 4** An example of a 3D model and its corresponding silhouette images. On the top is a 3D model downloaded from Google’s 3D Warehouse. For a bandwidth  $L = 3$ ,  $2L^2 = 18$  silhouettes will be rendered. In this figure, the top row corresponds to silhouettes from viewpoints with fixed colatitude ( $15^\circ$ ) but varying azimuth.

is defined generally for complex-valued functions. For real-valued functions the coefficient vectors  $(\hat{M}_m^l)_i$  exhibit an hermitian property:  $(\hat{M}_{-m}^l)_i = (-1)^m (\hat{M}_m^l)_i$ . These two facts show that only the coefficients  $(\hat{M}_m^l)_i$  for  $l$  even and  $m \geq 0$  are necessary, greatly reducing the storage space of our Fourier representation.

The Fourier representations of the two models,  $(\hat{M}_{1m}^l)_i$  and  $(\hat{M}_{2m}^l)_i$ , are the necessary input for evaluating the correlation similarity measure. From equation 9, we showed that the  $SO(3)$  Fourier coefficients of  $G_c(R)$  can be obtained in the spectral domain as:

$$\hat{G}_c^l = \sum_{i=1}^N \hat{M}_{1i}^l \overline{(\hat{M}_{2i}^l)^T} \quad (10)$$

To obtain the samples of our desired correlation function  $G_c(R)$ , we must take an inverse  $SO(3)$  Fourier transform as a final step. Note, we have the option of taking the inverse  $SO(3)$  transforms before or after the summation  $\sum_i$ . In other words, if we let  $\text{ISOFT}(\cdot)$  represent the inverse  $SO(3)$  Fourier transform operator,

the following are equivalent:

$$G_c(R) = \sum_{i=1}^N \text{ISOFT} \left( \hat{M}_{1_i}^l \overline{(\hat{M}_{2_i}^l)^T} \right) \quad (11)$$

$$= \text{ISOFT} \left( \sum_{i=1}^N \hat{M}_{1_i}^l \overline{(\hat{M}_{2_i}^l)^T} \right) \quad (12)$$

While these computations have numerically identical results, there is a clear advantage to equation 12. Evaluating equation 11 has  $O(NL^3 \log^2 L)$  complexity. This comes from having  $N$  separate  $SO(3)$  Fourier transforms, each of which has complexity  $O(L^3 \log^2 L)$ . On the other hand, evaluating equation 12 requires only one Fourier transform. Although the inner summation  $\sum_{i=1}^N$  over coefficient vectors has complexity  $O(NL^3)$ , the constant factor is minimal. The total complexity of equation 12 is  $O(NL^3) + O(L^3 \log^2 L) = O(L^3(\log^2 L + N))$ . In practice, the computational burden lies in the Fourier transform, and thus we see a speedup by a factor of approximately 10 when evaluating equation 12 in place of equation 11. We can also compare this complexity against the original definition of  $G_c(R)$  as given in equation 2. To evaluate equation 2 in the spatial domain would have a complexity of  $O(NL^5)$  (this would also be the complexity of evaluating [1] for similar numbers of silhouette and rotation samples).

In the final step, the maximum value from the samples of  $G_c(R)$  (as obtained via equation 12) is selected as the similarity score between the two input models.

#### 4.6 Sampling flexibility

We will now discuss how our approach addresses one of the key issues brought up earlier, namely the dependence between the number of silhouette viewpoint samples and the number of samples in the 3D rotation space. First, we note that our development allows for an arbitrarily dense sampling of the viewing sphere and 3D rotation space. For a fixed bandwidth  $L$  we will have  $2L$  silhouette viewpoint samples uniformly spaced in the each of the two spherical coordinates, as well as  $2L$  samples uniformly spaced in each of the three Euler angles. This straightforward formulation allows us to achieve a sampling where the maximum distance between any silhouette viewpoint and its nearest neighbor is arbitrarily small (similarly with 3D rotations), simply by varying the bandwidth  $L$ .

Furthermore, we can achieve an independence between the number of silhouette samples and the number of 3D rotations samples of  $G_c(R)$ . In other words, we are not forced to have the same bandwidth parameter  $L$  for both the silhouette model representation  $M(p)_i$  and the 3D correlation function  $G_c(R)$ . For example,

assume  $L'$  is the chosen bandwidth of the model representations  $M_{1,2}(p)_i$ , which implies a total of  $2L'^2$  silhouette images. Let  $L'' > L'$ . We can easily generate  $\hat{G}_c^l$  for  $l = 0, \dots, L'' - 1$  as in equation 10 by setting  $\hat{G}_c^l = 0, \forall L' \geq l < L''$ . In this approach, the extra samples obtained in the 3D rotation space by having a higher bandwidth  $L''$  are interpolated using the Fourier coefficients of  $M(p)_i$  up to bandwidth  $L'$ . Thus, our approach provides a simple mechanism for independently varying the number of silhouette viewpoint samples and the number of 3D rotation samples. If desired, many more samples of  $G_c(R)$  can be interpolated from few silhouette images. Contrast this to a direct spatial approach (e.g. [1]), where there are strict dependencies between silhouette view samples and possible 3D rotations, and no simple mechanism for interpolation exists.

## 5 A natural coarse-to-fine estimation of similarity

The development in the previous section presents a novel approach for determining the similarity between a pair of 3D models. Such a technique can be very important for an application such as 3D model retrieval, where the challenge is to identify the most similar models to a query from a very large database. In such a setting, it can be computationally infeasible to perform a full similarity evaluation between the query and every database model just to identify the few most similar models. Instead, when searching for nearest neighbors we would like to discard large numbers of candidate models with few computations. To this end, our model comparison approach can easily be extended to form an iterative coarse-to-fine evaluation of model similarity. The basic idea is very intuitive, and comes from the observation that the degree of a Fourier coefficient indicates the frequency component that is represented. In other words, a coarse estimation of similarity using only low-frequency signal information can be obtained by using only the low-degree Fourier coefficients. Subsequently, a higher precision can be achieved by introducing high-frequency signal information in the way of the high-degree Fourier coefficients. To build a 3D model retrieval system for a large database of models, we can proceed as follows:

In a pre-processing step, each model in the database is represented with the Fourier coefficients  $(\hat{M}_m^l)_i$  at some bandwidth  $L$ . Given a query model, the first iteration for retrieval involves evaluating a coarse similarity between the query and every database model. This coarse similarity is obtained by computing  $G_c(R)$  at some small bandwidth  $L' < L$ . Those models furthest from the query can be discarded. In each subsequent

iteration, a finer similarity score is computed between the query and remaining database candidates by evaluating  $G_c(R)$  at an increased bandwidth. In the final iteration a ranked list of nearest neighbors is created by evaluating  $G_c(R)$  at the full bandwidth  $L$  for the few remaining candidates. In this way we can discard the large majority of database models with limited computation.

## 6 Rotational invariants

The model comparison and retrieval approaches we have presented above utilize representations that are not invariant to 3D rotations. As we discussed earlier, a general alternative is to build rotational invariance directly into the model feature representation. Feature descriptors which are invariant to model transformations always lead to faster comparison (since no search over the transformation space needs to be done online), and are also suitable for use with standard off-the-shelf classification techniques (e.g. SVM classifiers). For sphere-based 3D model representations there are two ways to normalize for orientation. The simplest and most common approach is to align the model’s principal axes with a fixed reference frame. An alternative to this PCA-alignment is to identify the rotation-invariant terms in the spherical Fourier domain (see [2, 31] for details and other applications for such invariants). We saw earlier (equation 8) how the Fourier coefficients of a function transform under a 3D rotation of the original function. The Fourier analogue to 3D rotations are given by the matrix transformations  $U^l(R)$ . We know that these unitary transformations will not alter the distribution of spectral energy among coefficient degrees:

$$\|U^l(R)\hat{M}^l\|_2 = \|\hat{M}^l\|_2, \forall R \in SO(3)$$

where  $\|\cdot\|_2$  indicates  $L_2$  vector norm. We can build a rotation-invariant model feature vector by retaining only the magnitudes of the Fourier coefficient vectors ( $\|\hat{M}_i^l\|$ ). The total size of such a model descriptor is  $\lfloor \frac{L}{2} \rfloor N$ . For example, consider a model for which we render a very large number of silhouettes (e.g.  $L = 17$  means we must render  $2L^2 = 578$  images). Assuming  $N = 45$  as we have used throughout this paper, our model representation is just one feature vector of  $45 * 8 = 360$  dimensions. The distance between two models is defined as the Euclidean ( $L_2$ ) distance between their respective feature vectors.

## 7 Experiments

In this section we will study the effectiveness our proposed 3D model comparison technique with three chal-

lenging evaluations (the Princeton Shape Benchmark, the Shape Retrieval Contest in 2006, and a collection of models downloaded from Google’s 3D Warehouse). We begin with a study on the de-facto evaluation benchmark for 3D shape retrieval, the Princeton Shape Benchmark [32].

### 7.1 Princeton Shape Benchmark

The Princeton Shape Benchmark [32] provides a collection of 3D models designed for the standardized evaluation of retrieval, matching, clustering, and recognition algorithms. The database consists of 1814 manually categorized 3D models collected from the Web. The database is segregated into a training set consisting of 907 models and spanning 90 model classes, and a test set consisting of the remaining 907 models and spanning 92 model classes. In the test set, the largest category contains 26 models (“potted plant”), and the smallest category contains 4 models (there are 17 categories with just 4 models). Figure 5 shows a few examples of models in the benchmark.

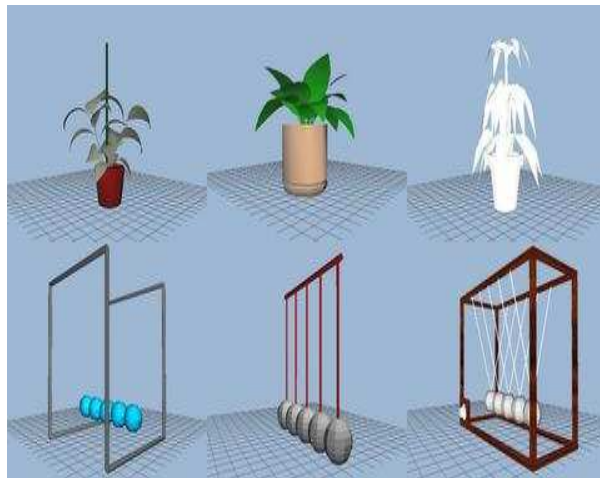


**Fig. 5** Thumbnail images of six different models in the Princeton Shape Benchmark [32]. The top row consists of thumbnails from the “potted plant” class, which constitutes the largest class in the PSB test set. The bottom row consists of thumbnails from the “Newtonian toy” class, which is one of 17 classes in the test set tied for having the fewest models (four).

To stay consistent with published evaluations on the benchmark, we restricted ourselves to evaluations over the 907 model test set. In principle, our approach is training-free, and thus could be evaluated over the entire 1814 model benchmark.

To evaluate the robustness of our method, we initialize every 3D model with a randomly generated 3D

rotation before rendering model silhouettes. This is important because although model orientation is unknown, it is quite common in the benchmark to see many models that are aligned with the ground plane in their native orientations. In order to provide a proper evaluation of our correlation-based method, a random rotation of each model will cancel out any orientation bias in the benchmark.

In general, evaluation over the test set is performed by removing one model to act as the query, and ranking the remaining models from most similar to least similar. This ranked list can be evaluated in a number of ways (a few of which we will detail below). Performance for a particular method or set of parameters is given by averaging the performance over all query models. The evaluation measures for the benchmark are as follows (see [32] for details):

1. *Nearest Neighbor* measures the accuracy of the first retrieved neighbor.
2. *First Tier* and *Second Tier*. The ratio of models in the query class that appear in the first  $K$  results. If  $|C|$  is the number of models in the query’s class,  $K = |C| - 1$  for first tier and  $K = 2 * (|C| - 1)$  for second tier.
3. *E-measure* is a combined measure of the precision and recall for a fixed number of results (here the evaluation neighborhood size is 32). The E-measure is defined as  $2 / (\frac{1}{P} + \frac{1}{R})$ , where precision (P) and recall (R) are defined in the usual document retrieval way.
4. *Discounted Cumulative Gain* (DCG) is an evaluation measure of the entire ranked list that weights positive results at the top of the list higher than positive results lower on the list.

The evaluation measures described above emphasize positive results earlier in the ranked retrieval. This is in line with the idea that for many search applications, users will often only be interested in the quality of the first few returned results. Perturbations towards the end of the list will have little effect on the perceived quality of the retrieval.

The performance criteria listed above were used to evaluate a number of existing 3D shape comparison and retrieval algorithms in [32]. We have reprinted these published results along with the performance of our proposed model similarity measure in table 1.

We ran the retrieval algorithm for 8 different bandwidth parameters, ranging from  $L = 3$  up to  $L = 17$ . In this setting, the selection of bandwidth was kept fixed for the entire algorithm (i.e. the same bandwidth  $L$  was used for feature generation and evaluating the correlation function  $G_c(R)$ ). Our evaluation indicates that we do see an improvement over the closest method,

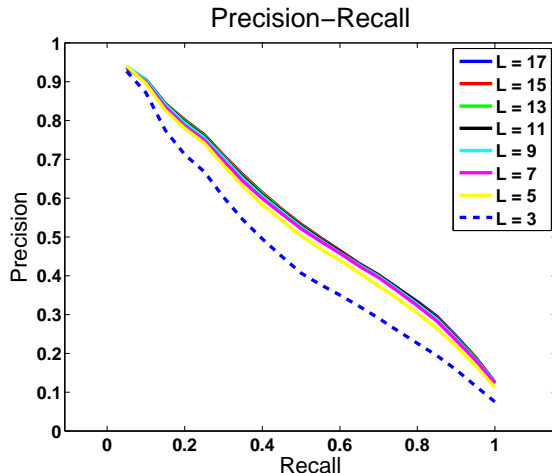


**Fig. 6** Precision-Recall curves for our proposed shape comparison algorithm on the Princeton Shape Benchmark test set. The evaluation code used to generate these plots was taken from the evaluation utilities provided with the benchmark [32]. As we can see, there is little variation in results between the lowest and highest bandwidths.

LFD [1]. Furthermore, we see close-to state of the art results at even lower bandwidth settings. Interestingly, the relative performance difference between retrievals run at the higher bandwidths ( $L \geq 9$ , for example) are very small. This fact can be clearly observed in figure 6, where we show precision-recall curves for the various bandwidth settings.

The gap in performance at various bandwidth settings indicates that our proposed coarse-to-fine scheme may prove just as effective as performing retrieval at the highest resolution of  $L = 17$ . What remains to be determined are the specifics of the incremental coarse-to-fine retrieval. Based on the results in table 1 and figure 6, we can do most of the ranking and similarity computation at the low bandwidths and use the high resolution bandwidth for a final “fine-tuning” (i.e. re-ranking) of a few models. What we would expect to see is that the DCG scores may not reach those of the highest bandwidth since DCG is a measure of the entire ranked listing. However, we would expect to see nearest-neighbor scores mostly unaffected.

We experimented with the following incremental scheme: first, the similarity scores are computed for all model pairs at the lowest bandwidth ( $L = 3$ ). In the second pass, we identify the most similar 20%, and re-rank these models by computing similarity at  $L = 5$ . In the third and final pass, we re-rank the 1% most similar models at  $L = 17$ . The results are shown in table 2. As expected, the global measurements like DCG fell somewhere between the low and high-bandwidth results. Surprisingly, however, the nearest-neighbor results outperformed all algorithms including the full  $L =$

| Shape Descriptor | Storage Size (bytes) | Discrimination (%) |            |             |           |      |
|------------------|----------------------|--------------------|------------|-------------|-----------|------|
|                  |                      | Nearest Neighbor   | First Tier | Second Tier | E-Measure | DCG  |
| <b>L=17</b>      | 27,630               | 67.3               | 41.2       | 50.2        | 29.6      | 65.9 |
| <b>L=15</b>      | 21,420               | 66.8               | 41.1       | 50.2        | 29.6      | 65.9 |
| <b>L=13</b>      | 16,200               | 66.7               | 40.8       | 50.1        | 29.5      | 65.7 |
| <b>L=11</b>      | 11,700               | 66.8               | 41.0       | 49.9        | 29.4      | 65.6 |
| <b>L=9</b>       | 7,920                | 66.8               | 40.6       | 49.8        | 29.4      | 65.5 |
| <b>L=7</b>       | 4,860                | 66.3               | 40.1       | 49.4        | 29.3      | 65.0 |
| LFD              | 4,700                | 65.7               | 38.0       | 48.7        | 28.0      | 64.3 |
| <b>L=5</b>       | 2,520                | 65.4               | 38.6       | 47.9        | 28.1      | 63.8 |
| REXT             | 17,416               | 60.2               | 32.7       | 43.2        | 25.4      | 60.1 |
| SHD              | 2,184                | 55.6               | 30.9       | 41.1        | 24.1      | 58.4 |
| GEDT             | 32,776               | 60.3               | 31.3       | 40.7        | 23.7      | 58.4 |
| <b>L=3</b>       | 900                  | 56.2               | 31.7       | 40.5        | 24.4      | 58.0 |
| EXT              | 552                  | 54.9               | 28.6       | 37.9        | 21.9      | 56.2 |
| SECSHEL          | 32,776               | 54.6               | 26.7       | 35.0        | 20.9      | 54.5 |
| VOXEL            | 32,776               | 54.0               | 26.7       | 35.3        | 20.7      | 54.3 |
| SECTORS          | 552                  | 50.4               | 24.9       | 33.4        | 19.8      | 52.9 |
| CEGI             | 2,056                | 42.0               | 21.1       | 28.7        | 17.0      | 47.9 |
| EGI              | 1,032                | 37.7               | 19.7       | 27.7        | 16.5      | 47.2 |
| D2               | 136                  | 31.1               | 15.8       | 23.5        | 13.9      | 43.4 |
| SHELLS           | 136                  | 22.7               | 11.1       | 17.3        | 10.2      | 38.6 |

**Table 1** Retrieval results of our proposed similarity measure, as well as a number of comparison methods, on the Princeton Shape Benchmark [32]. The rows denoted by “**L=**” correspond to evaluations of  $G_c(R)$  using different values for the bandwidth parameter  $L$ . In this evaluation, selection of  $L$  specifies the sampling in the silhouette viewpoint space as well as the 3D rotation space. The results for the competing algorithms are taken from [32]. The algorithms are sorted by the Discounted Cumulative Gain Score. The test data consists of 907 models classified into 92 categories. Surprisingly, even the low bandwidth correlations are outperforming most algorithms. See [32] for an overview of all the comparison algorithms.

| Nearest Neighbor | First Tier | Second Tier | E-Measure | DCG   |
|------------------|------------|-------------|-----------|-------|
| 67.5%            | 39.4%      | 48.0%       | 28.0%     | 64.7% |

**Table 2** Discrimination results for coarse-to-fine similarity computation. In this experiment three stages were used. First, all models were ranked according to similarity computed at  $L = 3$ . Subsequently, the best 20% of the ranked models were re-ranked with similarity computed at  $L = 5$ . In the final “fine-tuning” step, the closest 1% of the models were again re-ranked with similarity computed at  $L = 17$ . As expected, the global measurements like DCG fell somewhere between the low-res and high-res results. Surprisingly, however, the nearest-neighbor results outperformed all algorithms including the high-res computation.

17 evaluation. These results indicate that much of the work for retrieval is being done at the low frequencies. While the high-frequency model coefficients may not contribute as much to the overall scheme, they are very valuable as a “fine-tuning” mechanism for re-ranking the top results.

In addition to these quantitative results, we show some examples of the top retrieval results for various query models in table 3.

## 7.2 SHREC 2006

In addition to the extensive evaluation on the PSB, our correlation based shape retrieval algorithm was entered

into SHREC, the 3D Shape Retrieval Contest [33, 34] in 2006. The purpose of the contest was to study different retrieval methods under a wide variety of evaluation criteria. A set of 30 3D models served as the query set. The corpus against which ranked retrieval was to be performed was a permutation of the Princeton Shape Benchmark. The ranked retrieval lists for each of the 30 queries was evaluated in a number of ways. Individual per-query results were tabulated, as well as aggregate results over all 30 queries for each contest entry. In total, 17 aggregate evaluation criteria were used, and our proposed correlation method was the top performer in 11 of these 17 categories [33]. A subset of the aggregate results are shown in table 4. Qualitative results of our retrieval algorithm as it performed in this contest are shown in table 5. The table shows the 10 closest models in the database for 5 of the 30 queries used in the contest.

An alternative to the correlation-based comparison approach is to encode rotation-invariance directly into the feature descriptor. This can be done by computing rotation-invariant model descriptors as described in section 6. While the online comparison cost is much less (Euclidean distance of a small feature vector versus spherical correlation), the discrimination performance is expected to be much worse. This is in fact the observed effect in figure 7. Given a ranked list generated from rotation-invariant feature vectors, we observe how

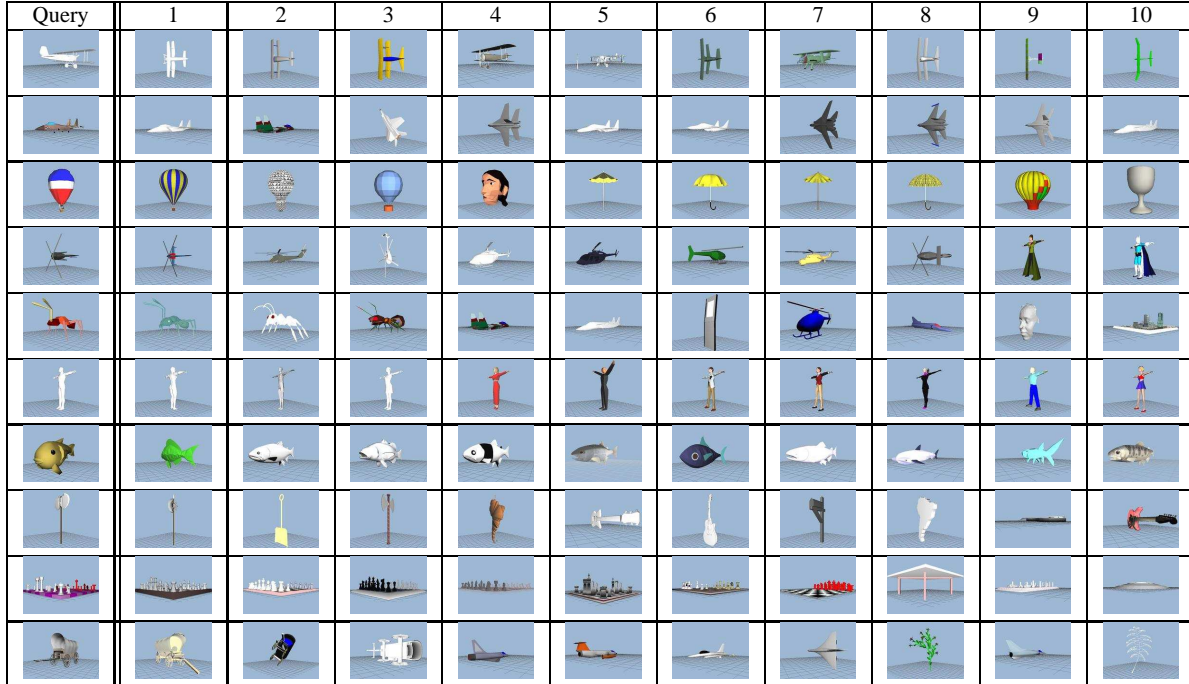


**Table 3** Retrieval results for 10 test queries in the Princeton Shape Benchmark (PSB). The first column shows each query’s thumbnail. The ten models to the right of each query are the closest models (in order) in the 907-model PSB test set.

| Shape Descriptor     | Mean Precision (highly relevant only) | Mean First Tier (highly relevant only) | Dynamic Average Recall | Normalized DCG at 5 | Normalized DCG at 50 |
|----------------------|---------------------------------------|--|------------------------|---------------------|----------------------|
| <b>L=17</b>          | 0.49                                  | <b>0.45</b>                            | <b>0.55</b>            | 0.68                | <b>0.58</b>          |
| Shilane et al [35]   | <b>0.54</b>                           | 0.41                                   | 0.50                   | 0.69                | 0.56                 |
| Zaharia et al [35]   | 0.50                                  | 0.39                                   | 0.50                   | 0.67                | 0.53                 |
| Daras et al [35]     | 0.45                                  | 0.43                                   | 0.52                   | <b>0.70</b>         | 0.56                 |
| Papadakis et al [35] | 0.44                                  | 0.42                                   | 0.50                   | 0.67                | 0.54                 |
| Chaouch et al [35]   | 0.40                                  | 0.38                                   | 0.50                   | 0.68                | 0.53                 |
| Laga et al [35]      | 0.23                                  | 0.24                                   | 0.33                   | 0.53                | 0.37                 |
| Jayanti et al [35]   | 0.17                                  | 0.17                                   | 0.27                   | 0.44                | 0.30                 |

**Table 4** A subset of the published results from SHREC2006 (3D Shape Retrieval Contest 2006) [33,35]. The results are averaged over the 30 test queries. For each query, the database models were manually labeled as highly relevant, marginally relevant, or irrelevant. The evaluation criteria follow the same definitions as with the evaluations for the Princeton Shape Benchmark, with a few exceptions. For a given query, if the recall ratio within the top  $i$  neighbors is given as  $r_i$ , then the Dynamic Average Recall is defined as the mean over all  $r_i$ . Normalized DCG represents the Discounted Cumulative Gain divided by the ideal or optimal possible Discounted Cumulative Gain score. For more contest results see [33, 35], and for a detailed explanation of the evaluation criteria see [34]. Each entrant into the competition was allowed multiple entries, either to be used for different algorithms, or just different parameter settings for the same general approach. To be fair to the comparison methods, we have only shown here the best performing method in each evaluation column for all the entrants. For our proposed method, we are showing the results at  $L = 17$ .

many of the top-ranked models must be observed before seeing 50% of the top  $K$  models retrieved using our correlation similarity measure (the plot shows the median over all 30 queries). For example, in order to see 50 of the top 100 retrieved models using a correlation similarity, we have to examine the first 213 retrieved models using rotation-invariant descriptors. As expected, the computational benefit of building invariance directly into the descriptor is offset by the loss in discrimination power.

### 7.3 Google 3D Warehouse

While the Princeton Shape Benchmark has become one of the standard evaluation datasets for 3D model retrieval algorithms, the benchmark can be criticized for its lack of variation within classes in addition to other factors such as a lack of articulated object classes. We therefore evaluated our proposed model comparison method on a more challenging real-world dataset. This set consists of 772 3D models downloaded from Google’s 3D

| Query | 1 | 2 | 3 | 4 | 5 | 6 | 7 | 8 | 9 | 10 |
|-------|---|---|---|---|---|---|---|---|---|----|
|       |   |   |   |   |   |   |   |   |   |    |
|       |   |   |   |   |   |   |   |   |   |    |
|       |   |   |   |   |   |   |   |   |   |    |
|       |   |   |   |   |   |   |   |   |   |    |
|       |   |   |   |   |   |   |   |   |   |    |

**Table 5** Top 10 retrieval results for 5 of the 30 queries from the SHREC 2006 contest. On the left column we show the query models, and to the right of each query model are the 10 nearest neighbors in the database.

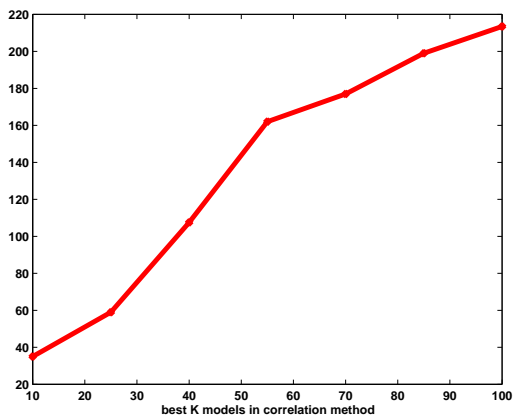


**Fig. 7** This plot shows how many models in the ranked list (obtained by comparing rotation-invariant vectors) you need to traverse before finding 50% of the best  $K$  matches in the ranked list obtained with the proposed correlation scheme. The plot shows the median over all test queries. For example, 50% of the best 100 matches from the correlation method will appear in the first 213 matches from the ranked list obtained by comparing rotation-invariant model descriptors.

Warehouse, which is a repository for 3D models on the Web. All the models are grouped into a total of 25 classes. The categorization of models corresponds simply to the search term used to find and the model. The largest category is “airplane” with 58 models, and the smallest is “fish” with only 6 models.

Figure 8 shows a few examples from the dataset. One of the biggest challenges posed by this repository is that individual model files can consist of multiple objects. For example, the figure shows that the “garage” model consists of multiple structures in addition to the garage object (such as the ground plane).

Our primary evaluation criteria for this set was precision versus recall. We averaged results over individual classes, as well as over all 772 models. For comparison, we evaluated the method proposed by [13], where

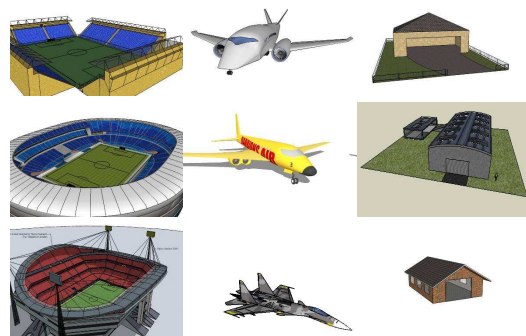


**Fig. 8** Samples of the 3D model dataset created from 3D Warehouse. Each column shows samples from a single category. The three categories shown here are “stadium”, “plane”, and “garage”. These sample images indicate a few reasons why this collection is very challenging. For example, we see that there is a large variation in scale and complexity within and between categories. Also, models on 3D Warehouse are not just individual objects as in the Princeton Shape Benchmark. Here individual model files such as the garage can consist of multiple pieces like the garage, ground plane, etc. This makes matching based solely on shape content very challenging.

3D Zernike descriptors are used to represent the models. Note, for this dataset all of our similarity measure evaluations are performed at  $L = 11$ . Results averaged per class are shown in figure 9, while results averaged over all the models are shown in figure 10. The results indicate consistently high performance for most classes of models in the set.

#### 7.4 Timings

The algorithms proposed in this paper can play a big role in a system for 3D model search and retrieval. Hence, it is important to be aware of the execution times. There are two stages of computation. The pre-processing stage involves computing the model features. This is an offline step regarding database cre-

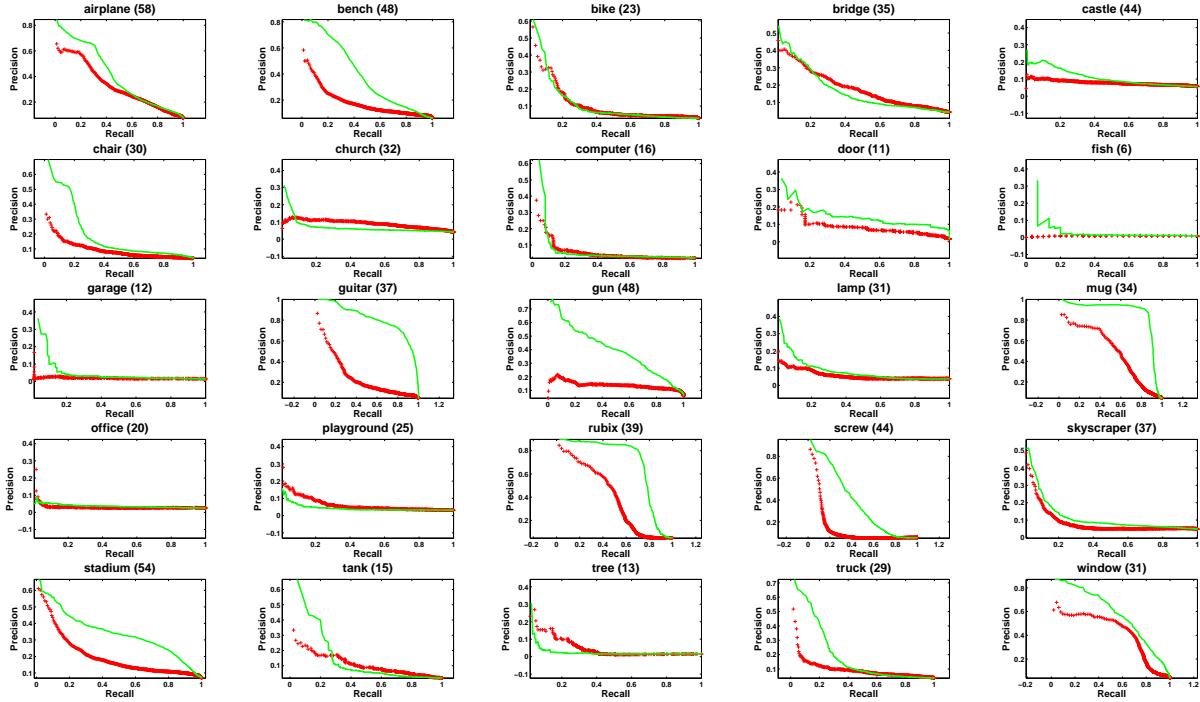


**Fig. 9** Precision versus recall curves for each of the 25 classes of models in the 3D Warehouse dataset. The number of models in each class appears in parentheses next to the class name. The solid green line is the curve from our proposed method with bandwidth setting  $L = 11$ . The red line is the curve of the method proposed in [13].

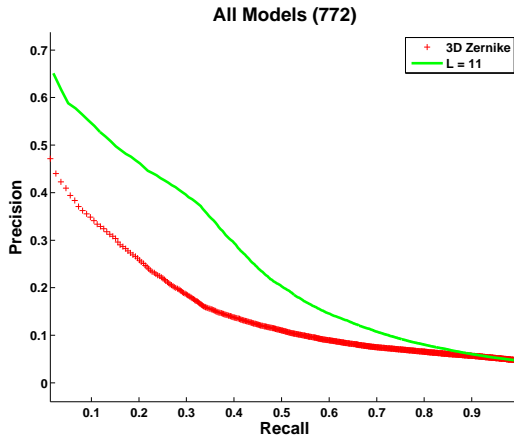


**Fig. 10** Precision versus recall curves averaged over all the models in the 3D Warehouse dataset. The total number of models in the dataset is 772. The solid green line is the curve from our proposed method with bandwidth setting  $L = 11$ . The red line is the curve of the method proposed in [13].

ation, but the computation time is still important since the query models may not have been seen before. In our algorithm feature generation involves generating model silhouettes, extracting features from the silhou-

ettes, and then performing a spherical Fourier transform. For the highest resolution we tested in this paper (bandwidth  $L = 17$ , which corresponds to 578 silhouettes), the total silhouette feature extraction time was on average 1.58 seconds. Since our feature vectors are 45 dimensional, we must take 45 Fourier transforms, for which the total time is 0.0042 seconds. The remaining preprocessing piece is generating the silhouettes. In figure 11 we show the time it takes to render all the silhouettes for one model. As expected, the times are dependent on the number of polygons. For models with relative few polygons (e.g. 20,000), the rendering time is about one second. For models with over 300,000 polygons the rendering time is almost three seconds (for 578 silhouettes). However, the OpenGL code used for this process is far from optimized and does not take advantage of the many options available with modern graphics cards, so there remains room for improvement.

The online cost of the model comparison algorithm is the computation time required to estimate the correlation function  $G_c(R)$  and identify the maximum value. Timings for evaluating equation 12 at various bandwidth settings, as well as a comparison with [1], are

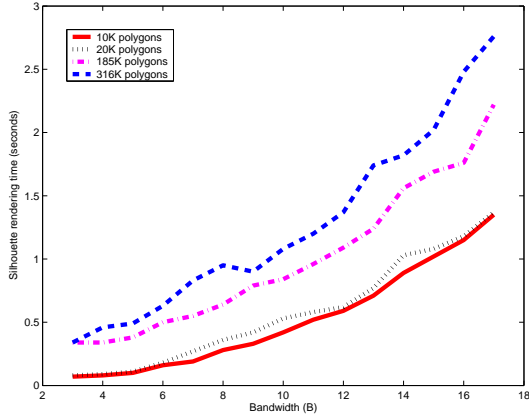


**Fig. 11** Silhouette rendering times for various bandwidths and model sizes. For a bandwidth  $L$ , the number of silhouettes rendered is  $2L^2$ . For example, it takes less than 3 seconds to generate 578 silhouettes of a model with 316K polygons.

| Method      | Time (s) |
|-------------|----------|
| <b>L=3</b>  | 0.00005  |
| <b>L=5</b>  | 0.00008  |
| <b>L=7</b>  | 0.00058  |
| <b>L=9</b>  | 0.00113  |
| <b>L=11</b> | 0.00375  |
| <b>L=13</b> | 0.00672  |
| <b>L=15</b> | 0.00512  |
| <b>L=17</b> | 0.017825 |
| LFD [1]     | 0.0208   |

**Table 6** Time in seconds to obtain a similarity score between two models given their precomputed model feature representations. The top rows give times for different bandwidths, which represent different levels of precision and resolution. The bottom row gives the timing for an implementation of direct silhouette feature comparison as given in [1]. This computation involves computing the  $L_1$  distance between collections of 10 silhouette feature vectors over a total of 5460 possible rotational alignments. An optimized implementation timing (e.g., using lookup tables) was reported as 0.0013 seconds in [32]. The closest setting of ours is  $L = 7$ , which uses 98 silhouette images, whereas 100 silhouettes are needed in [1]. Our approach (0.00058s,  $L = 7$ ), is significantly faster than either LFD implementation (0.0208s, our implementation, and 0.0013s optimized implementation).

given in table 6. The machine used to generate these timings is a Apple Powerbook laptop computer with 2GB of RAM.

## 8 Conclusion

In this paper we presented a new similarity measure for comparing 3D shapes based on a visual representation, as well as a novel estimation technique for the efficient evaluation of the similarity measure. We showed how an analysis in the spherical Fourier domain provides a flexibility to all components of our formulation, and

can also lead to a very intuitive and effective coarse-to-fine 3D model retrieval system.

A thorough evaluation on multiple benchmarks shows our proposed methods combine the discriminative power of a visual model representation with efficient computation.

## 8.1 Acknowledgments

We thank Corey Goldfeder for the implementation of the 3D Zernike descriptors described in [13].

## References

1. D.-Y. Chen X.-P. Tian, Y.T.S., Ouhyoung, M.: On visual similarity based 3D model retrieval. In: Eurographics (2003)
2. Kazhdan, M., Funkhouser, T., Rusinkiewicz, S.: Rotation invariant spherical harmonic representation of 3D shape descriptors. In: Symposium on Geometry Processing (2003)
3. Vranic, D.V.: An improvement of rotation invariant 3D shape descriptor based on functions on concentric spheres. In: Proceedings of International Conference on Image Processing, pp. 757–760 (2003)
4. Saupe, D., Vranic, D.V.: 3D model retrieval with spherical harmonics and moments. In: Proceedings of the 23rd DAGM-Symposium on Pattern Recognition, pp. 392–397. Springer-Verlag, London, UK (2001)
5. Ankerst, M., Kastenmüller, G., Kriegel, H.P., Seidl, T.: Nearest neighbor classification in 3D protein databases. In: Proceedings of the Seventh International Conference on Intelligent Systems for Molecular Biology, pp. 34–43. AAAI Press (1999)
6. Kang, S.B., Ikeuchi, K.: Determining 3-D object pose using the complex extended gaussian image. In: Proceedings of the 1991 IEEE Computer Society Conference on Computer Vision and Pattern Recognition (CVPR '91) (1991)
7. Horn, B.K.P.: Extended gaussian images. *IEEE* **72**, 1671–1686 (1984)
8. Osada, R., Funkhouser, T., Chazelle, B., Dobkin, D.: Matching 3D models with shape distributions. In: SMI '01: Proceedings of the International Conference on Shape Modeling & Applications, pp. 154–166. IEEE Computer Society, Washington, DC, USA (2001)
9. Ohbuchi, R., Osada, K., Furuya, T., Banno, T.: Salient local visual features for shape-based 3D model retrieval. In: IEEE International Conference on Shape Modeling & Applications (2008)
10. Ohbuchi, R., Minamitani, T., Takei, T.: Shape-similarity search of 3D models by using enhanced shape functions. In: TPCG '03: Proceedings of the Theory and Practice of Computer Graphics, p. 97. IEEE Computer Society, Washington, DC, USA (2003)
11. Tangelder, J.W., Veltkamp, R.C.: A survey of content based 3d shape retrieval methods. *Multimedia Tools Appl.* **39**(3), 441–471 (2008)
12. Makadia, A., Visontai, M., Daniilidis, K.: Harmonic silhouette matching for 3D models. In: 3DTV. Kos (2007)
13. Novotni, M., Klein, R.: 3D zernike descriptors for content based shape retrieval. In: SM '03: Proceedings of the eighth ACM symposium on Solid modeling and applications, pp. 216–225. ACM, New York, NY, USA (2003). DOI <http://doi.acm.org/10.1145/781606.781639>

14. Johnson, A.E., Hebert, M.: Using spin images for efficient object recognition in cluttered 3D scenes. *IEEE Trans. Pattern Anal. Mach. Intell.* **21**(5), 433–449 (1999)
15. Johnson, A.: Spin-images: A representation for 3-D surface matching. Ph.D. thesis, Robotics Institute, Carnegie Mellon University, Pittsburgh, PA (1997)
16. Frome, A., Huber, D., Kolluri, R., Bulow, T., Malik, J.: Recognizing objects in range data using regional point descriptors. In: *Proceedings of the European Conference on Computer Vision (ECCV)* (2004)
17. Kortgen, M., Park, G.J., Novotni, M., Klein, R.: 3D shape matching with 3D shape contexts. In the 7th Central European Seminar on Computer Graphics (2003)
18. Belongie, S., Malik, J., Puzicha, J.: Shape matching and object recognition using shape contexts. *Pattern Analysis and Machine Intelligence, IEEE Transactions on* **24**(4), 509–522 (2002)
19. Lowe, D.G.: Object recognition from local scale-invariant features. In: *ICCV '99: Proceedings of the International Conference on Computer Vision-Volume 2*, p. 1150. IEEE Computer Society, Washington, DC, USA (1999)
20. Funkhouser, T., Min, P., Kazhdan, M., Chen, J., Halderman, A., Dobkin, D., Jacobs, D.: A search engine for 3D models. *ACM Transactions on Graphics* **22**(1), 83–105 (2003)
21. Thurston, W.P.: *Three-Dimensional Geometry and Topology*. Princeton University Press (1997)
22. Zhang, D.S., Lu, G.: An integrated approach to shape based image retrieval. In: *Proc. of 5th Asian Conference on Computer Vision (ACCV)*, pp. 652–657. Melbourne (2002)
23. Burel, G., Henoco, H.: Determination of the orientation of 3D objects using spherical harmonics. *Graph. Models Image Process.* **57**(5), 400–408 (1995)
24. Kostelec, P.J., Rockmore, D.N.: FFTs on the rotation group. In: *Working Paper Series*, Santa Fe Institute (2003)
25. Makadia, A., Daniilidis, K.: Rotation recovery from spherical images without correspondences. *IEEE Trans. Pattern Anal. Mach. Intell.* **28**(7), 1170–1175 (2006)
26. Kazhdan, M.: An approximate and efficient method for optimal rotation alignment of 3D models. *IEEE Trans. Pattern Anal. Mach. Intell.* **29**(7), 1221–1229 (2007). DOI <http://dx.doi.org/10.1109/TPAMI.2007.1032>
27. Kovacs, J.A., Wriggers, W.: Fast rotational matching. *Biological Crystallography* **58**, 1282–1286 (2002)
28. Makadia, A., Sorgi, L., Daniilidis, K.: Rotation estimation from spherical images. In: *ICPR '04: Proceedings of the Pattern Recognition, 17th International Conference on (ICPR'04) Volume 3*, pp. 590–593. IEEE Computer Society, Washington, DC, USA (2004)
29. Arfken, G., Weber, H.: *Mathematical Methods for Physicists*. Academic Press (1966)
30. Driscoll, J., Healy, D.: Computing fourier transforms and convolutions on the 2-sphere. *Advances in Applied Mathematics* **15**, 202–250 (1994)
31. Makadia, A., Daniilidis, K.: Direct 3D-rotation estimation from spherical images via a generalized shift theorem. In: *IEEE Conf. Computer Vision and Pattern Recognition*. Wisconsin, June 16-22 (2003)
32. Shilane, P., Min, P., Kazhdan, M., Funkhouser, T.: The princeton shape benchmark. In: *Shape Modeling International*. Genova, Italy (2004)
33. AIM@SHAPE: <http://give-lab.cs.uu.nl/shrec/shrec2006/> (2006)
34. Typke, R., Veltkamp, R.C., Wiering, F.: Evaluating retrieval techniques based on partially ordered ground truth lists. In: *Proceedings International Conference on Multimedia & Expo* (2006)
35. Veltkamp, R.C., Ruijsenaars, R., Spagnuolo, M., van Zwol, R., ter Haar, F.: *Shrec2006 3d shape retrieval contest*. technical report, Utrecht University (2006)